Thermal treatment of W large-scale fiberform nanostructures

Shin Kajita*
Institute of Materials and Systems for Sustainability, Nagoya University, Nagoya 464-8603, Japan

Tatsuki Okuyama and Hirohiko Tanaka, Tatsuya Kuwabara, Noriyasu Ohno
Graduate School of Engineering, Nagoya University, Nagoya 464-8603, Japan

Naoaki Yoshida
Research Institute for Applied Mechanics, Kyushu University, Kasuga, Fukuoka 816-8580, Japan
(Dated: December 7, 2021)

Recent experiments have revealed that accelerated tungsten (W) nanostructure growth occurs during the exposure to helium (He) plasmas with an additional W deposition, and mm-thick large-scale fiberform nanostructures (LFNs) are formed when certain condition is satisfied. In order to reveal whether accelerated growth occurs in fusion device, it is important to understand the annealing process in addition to the growth process. In this study, we will perform thermal treatment of W LFNs. Detailed observation reveals that the LFNs shrink at a faster rate than that of conventional fuzz, though it takes longer time to fully be reintegrated to the surface because the thickness is orders of magnitude greater.

I. INTRODUCTION

Tungsten (W) is a leading candidate material for plasma facing components in fusion devices because of its low sputtering yield and low tritium inventory. However, it has been recognized that the thermal and physical properties are significantly altered by the exposure to helium (He) plasmas, especially when fiberform nanostructures called *fuzz* are grown on the surface [1–5]. Concerning the fuzz growth, an acceleration in the growth rate has been recently identified with additional W deposition, and mm-thick large scale fiberform nanostructures (LFNs) are grown on the surface when a certain set of conditions is satisfied [6]. The acceleration in the growth rate has been identified in a magnetron sputtering device [7] in addition to linear plasma devices (NAGDIS-II [6] and Magnum-PSI [8]).

To answer the question whether fuzz is grown in fusion relevant conditions, it is important to discuss the counter-growth effects such as sputtering [9–11] and annealing [12–15] in addition to growth process [16]. Concerning the conventional fuzz growth, De Temmerman *et al* have considered those effects and showed that $\sim$1-μm-thick fuzz can be grown under fusion relevant condition, and that the energy of edge localized modes (ELMs) [17] is a key parameter for the fuzz growth [18]. However, thermal response of thick fuzzy layer formed with deposition including LFNs has yet to be fully understood. In this study, we perform thermal treatment and investigate morphology changes, annealing rate, and He desorption behavior of thick W fuzzy layer including LFNs formed under deposition conditions.

II. EXPERIMENTAL SETUP

Samples were prepared in the linear divertor simulator NAGDIS-II, where a $\sim$2-m-long cylindrical plasma is formed by a direct current arc discharge. A substrate is installed in the downstream of the steady state He plasma. Adjacent to the substrate, a sputtering wire, which was biased to $V_{\rm sw} < -200$ V, was introduced to sputter W atoms from the sputtering wire and deposit them to the substrate. The detailed description of the setup of the deposition experiments are found in elsewhere [6]. The substrate is exposed to the He plasma while sputtered particles from the sputtering wire deposit on the surface. The substrate surface is parallel to the magnetic field line. Since an ion sheath is formed around the substrate, ions are always bombarded almost from the normal direction of the surface. Thermal treatment of the prepared samples is performed in two different devices: a heating stage in transmission electron microscope (TEM) for in-situ observation ($\leq$1273 K) and a thermal desorption spectroscopy (TDS) device where the sample temperature can be increased in a controlled manner in vacuum. In the TDS device, the temperature was increased to 1473-1673 K at a ramp rate of 0.5 K/s and kept for 30 min at maximum temperatures. We also analyzed the He desorption behavior during the annealing process.

* kajita.shin@nagoya-u.jp

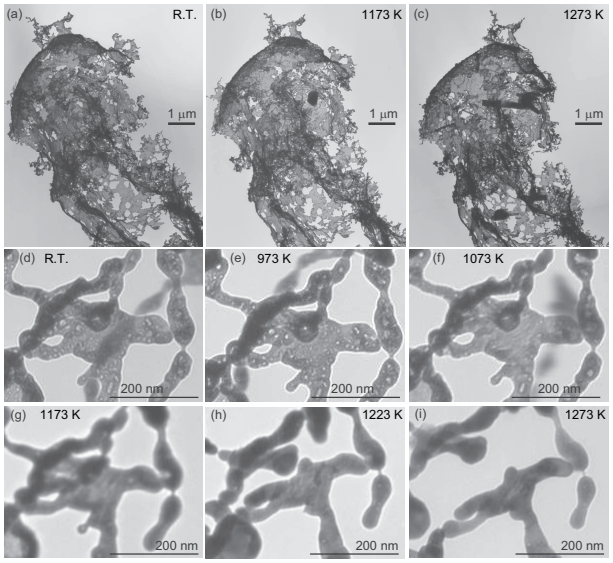

FIG. 1. TEM images of LFN while being heated in TEM using a heating stage. The temperature when the image was taken is at (a,d) R.T, (e) 973 K, (f) 1073 K, (b,h) 1173 K, (i) 1223 K, and (c,j) 1273 K.

III. THERMAL TREATMENT

A. In-situ TEM observation (up to 1273 K)

Figure 1 shows TEM images of a part of W LFN observed in-situ using a heating stage in the TEM device. The sample temperature was increased from room temperature (RT) to 1273 K as stepwise, and observations were made while the sample temperature was kept at 573, 673, 773, 873, 973, 1073, 1173, 1223, and 1273 K for 15-20 min. The LFNs were formed on a half circular W sample 3 mm in diameter, which can be installed directly to a TEM stage without additional milling or coating. In Fig. 1(a-c), low magnification TEM images at RT, 1173 and 1273 K, respectively, are shown. The 10-μm tall structure is made of membrane with holes and nanofibers. In this scale, no significant changes are identified by the thermal treatment. Figure 1(d-i) are TEM images with larger magnifications at RT, 973, 1073, 1173, 1223, and 1273 K, respectively. Although many He bubbles are observed inside the membrane and fibers up to 973 K, the number of bubbles decreases from 1073 K. The bubbles are still identified at 1273 K, but the number decreases significantly. Membrane part located around the image center started to shrink from 1173 K, and only fibers remained in the image in Fig. 1(j).

B. Higher temperature annealing

Figure 2(a-d) shows SEM images of LFNs before and after annealing at 1473, 1573, and 1673 K, respectively. The diameter of the fiber became thicker with increasing the annealing temperature. It is thought that the W surface diffusion, which becomes more active with increasing T_s, occurs on the fibers, causing the fiber diameter to be larger, as was observed on the annealing of conventional fuzz [19]. It is noted that even at the thermal treatment of 1673 K, the fiberform nanostructures remained on the surface, while the fiber width increased. There were many He bubbles in fibers before annealing, as shown in Fig. 1(d); recent TEM observation have revealed that there were no He bubbles in fibers after the annealing at 1673 K [20]. As far as we know, it has yet to be understood why such a significant change occurs during annealing even if the temperature is less than half the melting point. In this paper, we focused on the change in the thickness of the fuzzy material during annealing and compared to an empirical model of the fuzz thickness during annealing based on available data from many literatures [18].

SEM analysis in Fig. 2 focused on a part of LFNs (visibly identified structures), which covers half or less than that of the sample. From here, we focus on the annealing effect of the deposition layer without the visible LFNs (hereafter we will refer to this part as the base part of the sample). Figure 3 shows cross sectional SEM micrographs of the base part of the sample before and after annealing. The sample was exposed to the plasma with W deposition at $T_s = 1310 - 1340$ K and $V_{\rm sw} = -400$ V up to the He fluence of 5.6-6.1$\times 10^{25}$ m^{-2}, and LFNs were formed on the surfaces. Initially, the height of the fuzzy layer on the base part was $\approx$10 μm (Fig. 3(a)). We can say that an

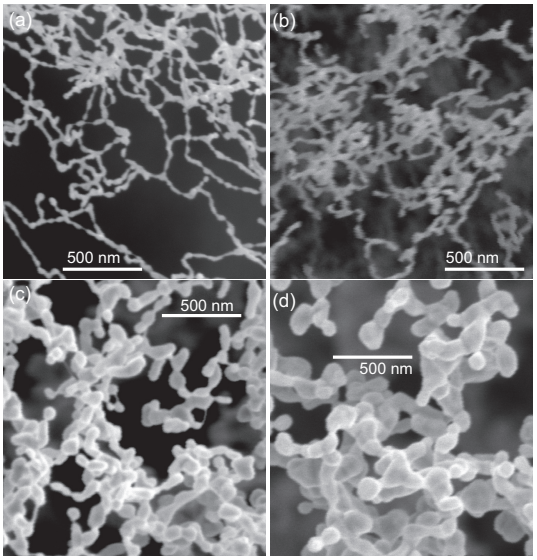

FIG. 2. SEM images of LFNs (a) before and (b-d) after annealing. The annealing temperature is (b) 1473 K, (c) 1573 K, and (d) 1673 K.

enhanced fuzz growth at an order of magnitude faster growth rate occurred with deposition, considering the fact that the thickness of conventional fuzz layer, which can be well characterized by the He fluence, would be $\sim$1 μm without deposition at the He fluence of $\sim 5 \times 10^{25}$ m^{-2} [16, 21]. This is similar to the cases identified in Magnum-PSI device [8]. When the annealing temperature was 1473 K (Fig. 3(b)), the fuzz layer thickness did not change at all. At 1573 K (see in Fig. 3(c)), the layer shrunk a little by $\approx$1 μm, and it decreased significantly to 1 μm at 1673 K (see in Fig. 3(d)).

The temperature dependent diffusion-like coefficients of annealing were obtained in two different temperature ranges based on the review of available experimental data [18]. The dotted curve in Fig. 3(e) shows the diffusion-like coefficient of annealing, D_{anneal}, obtained from the fitting shown in Ref. [18], and black squares show some experimental data close to the temperatures used in this study [12, 14, 15]. The diffusion-like coefficient is obtained from the following relation of the height of the fuzzy layer

$$h_{\mathrm{fuzz}}(t) = h_{\mathrm{fuzz}}(0) - (2D_{\mathrm{anneal}}t)^{1/2}, \tag{1}$$

where $h_{\mathrm{fuzz}}(t)$ is the height of fuzzy layer after annealing for t. Red circles show the obtained D_{anneal} from the samples in this study. The result suggests that D_{anneal} is higher than that of fuzz cases especially at 1673 K.

One of the major differences is that the initial thickness of the fuzzy layer is $\approx$10 μm, which is much thicker than that in the previous studies. Considering that LFNs were also reduced greatly from the initial height of a mm range, the change in height during annealing may not necessarily be controlled by a diffusion limited process. One of the influential factors would be the difference in porosity. The porosity increases with increasing the height of the fuzzy layer [9] and that of the LFNs is an order magnitude higher value than that of conventional fuzz [22]. The annealing rate can increase with increasing the porosity even at the same temperature. It is noted that the high porosity of LFN is mainly due to the spaces between fibers and does not directly reflect the vacancies inside material. Thus, it is unlikely that the porosity is an influential factor for the He contents to be discussed next.

C. He desorption

He desorption behavior was measured using the TDS device shown in Fig. 4(a). We calibrated the absolute He desorption by using VSLC leak standards (Artisan Technology Group). Figure 4(b) shows He desorption rate as a function of the sample temperature for three samples: (i) a conventional fuzz sample (blue), (ii) an LFN sample after removing the LFN part (red), and (iii) an LFN sample (black). Concerning sample (ii), we wiped the sample with a waste paper sheet (Kimwipe) without touching the bulk surface. The visible mm-thick fur-like structure was so fragile that they were removed mostly, but the base part of deposition layer (10-μm-thick fuzzy layer) remained as it was. From all the samples, in addition to the peak around 350 K, which is from weak trapping sites such as distorted lattice around He bubbles [23], strong desorption starts from 800 K and peaks around 1000-1300 K. In general, for

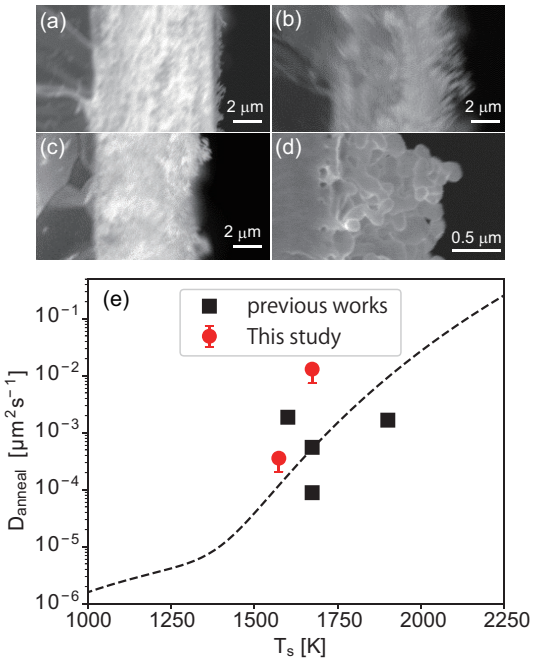

FIG. 3. Cross sectional SEM micrograph of the samples (a) before annealing and (b-d) after annealing at 1473, 1573, and 1673 K, respectively, and (e) diffusion like coefficient for annealing D_{anneal} from Ref. [18] (dotted line), annealing experiments of fuzz [12, 14, 15] (black markers), and the data in this study (red makers). The annealing could occur during the ramping at lower annealing rates; we considered the effect by adding half of the ramp time and showed with a half error bar.

fuzzy samples, because the desorption peak altered significantly by ramping rate of temperature and from sample to sample, we cannot say that the difference in the peak between the three samples is significant. However, the amount of desorption is considerably different. Figure 4(c) summarizes the total He desorption up to 1473 K for six different samples: samples (i)-(iii) in Fig. 4(b) and three additional LFN samples (iv)-(vi). We should say that He desorption above 1473 K is not negligible as it was continued to be released even at 2000 K [24]. Comparing from the He content on fuzzy W samples measured by elastic recoil detection (ERD) [25] and nuclear reaction analysis (NRA) [26], it was less than half of them on sample (i). Thus, since the total He desorption can be two to three times greater, we will focus on the relative variation in the He desorption between the samples. Also, there is a variance in the He desorption amount, and the difference can be identified from the comparison between (iii)-(vi). The difference in the He desorption between the four LFN samples (sample (iii)-(vi)) is not significant even if the He fluence is increased by ≈80% from sample (vi) to (iii). The He desorption decreased by ∼30% when removing LFNs (sample (ii)). Furthermore, the He desorption from LFN samples (sample (iii)-(vi)) is roughly 2.5 times greater than that of fuzzy sample (sample (i)).

The He desorption on sample (ii) increased by 90% from that of sample (i). Doerner *et al.* showed that the majority of He was identified below the fuzzy layer using NRA measurement [26]. However, the increase from sample (i) to (ii) indicates that the total He content in the fuzzy layer is comparable or greater than that below the fuzz on sample (ii). One of the causes is likely in the difference in the thickness of fuzzy layer. In Ref. [26], the thickness of the fuzzy layer was likely to be ∼3 μm because the He fluence was 3×10^{26} m^{-2} [16], and the He content on fuzz was estimated to be 30-40% of that in the fuzz removed region. In this study, the thickness of fuzzy layer is ∼1 and 10 μm for sample (i) and (ii), respectively, and the He desorption increased by 90% from sample (i) to sample (ii). Considering the above facts, the ratio of the He content in fuzz region would increase almost in proportion to the thickness of the fuzzy layer, and 1-μm-thick fuzzy layer contains roughly 10% of that below the fuzzy layer. In other words, He content on the sample increases with the fuzzy layer thickness, and the major storage of He gradually shifts to fuzzy layer when the fuzzy layer thickness is greater than 10 μm. In the future, it is expected to investigate the retention of hydrogen isotopes in the thick fuzzy layer formed by deposition.

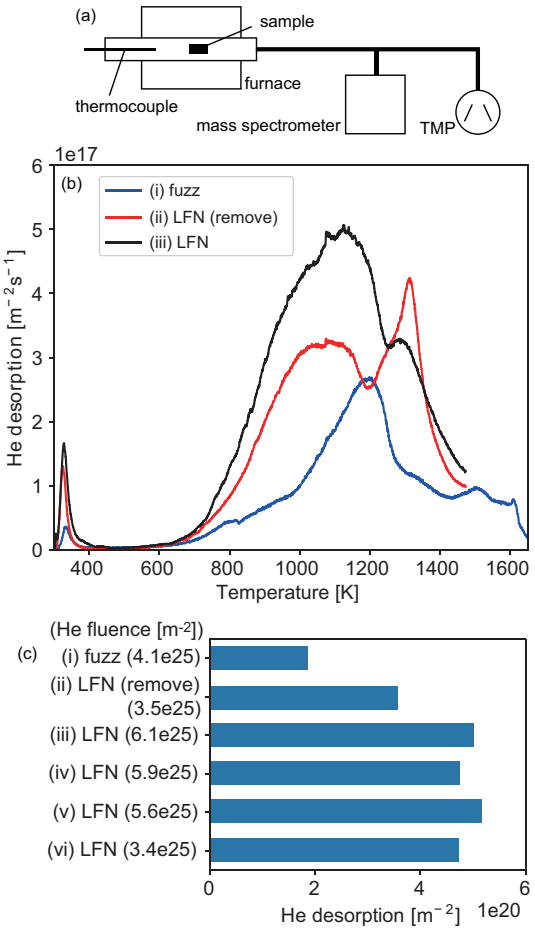

FIG. 4. (a) A schematic of the TDS device, (b) He desorption rate as a function of the sample temperature for samples (i)-(iii), and (c) a summary of total He desorption up to 1473 K for samples (i)-(vi). The samples (i) is a conventional fuzz sample, sample (ii) is an LFN sample after removing the LFN part, and samples (iii)-(vi) are LFN samples at different He fluences.

IV. CONCLUSIONS

Thermal treatment of tungsten large-scale fiberform nanostructures (LFNs), which was formed by the exposure to helium (He) plasmas with additional deposition, was performed, and changes in morphology and He content were investigated. In-situ TEM observation of LFNs during the thermal treatment up to 1273 K found that the overall shape of LFNs did not change at all, while the He bubbles gradually disappeared from the nanofibers. The width of the nanofibers apparently changed during the thermal treatment at 1573 K for 30 min, and almost no He bubbles existed after the thermal treatment at 1673 K for 30 min while the width of the fiber grew to 100-200 nm. The annealing rate of the fuzzy layer was deduced from the change in the layer thickness as focusing on the position where LFNs did not cover. It is noted that the fuzzy layer thickness was 10 μm before the annealing, which was way greater than that without deposition. It was found that the annealing rate at 1573 K was comparable to but was considerably higher at 1673 K than that of conventional fuzz. Also, thermal desorption spectroscopy analysis showed that He retention of LFN samples had more than twice greater than that of conventional fuzzy sample. The results suggested that He content increases with the fuzzy layer thickness and can exceed that in the layer below the fuzz when a thick ($\geq$10 μm) fuzzy layer is formed. In other words, the major storage of He will gradually shift to the fuzzy layer when the fuzzy layer increases to greater than 10 μm. It is interest to investigate the release of He in response to transients from the thick fuzzy layer and retention of hydrogen isotopes in the layer for the future. It has been assumed that the annealing rate is constant in time. However, the annealing rate may vary with changing the parameters such as porosity and thickness; it is of interests to measure the thickness of the LFN during annealing in future.

ACKNOWLEDGEMENT

The authors thank Mr. S. Kawaguchi for preparation of some LFN samples for thermal treatment. This work was supported in part by a Grant-in-Aid for Scientific Research 19H01874, and Fund for the Promotion of Joint International Research 17KK0132 from the Japan Society for the Promotion of Science (JSPS).

[1] M. Baldwin and R. Doerner: Nucl. Fusion **48** (2008) 035001 (5pp).
[2] S. Kajita, W. Sakaguchi, N. Ohno, N. Yoshida and T. Saeki: Nucl. Fusion **49** (2009) 095005.
[3] G. De Temmerman, K. Bystrov, J. J. Zielinski, M. Balden, G. Matern, C. Arnas and L. Marot: Journal of Vacuum Science & Technology A **30** (2012) 041306.
[4] K. D. Hammond: Materials Research Express **4** (2017) 104002.
[5] F. W. Meyer: Journal of Physics B: Atomic, Molecular and Optical Physics **52** (2019) 012001.
[6] S. Kajita, S. Kawaguchi, N. Ohno and N. Yoshida: Sci. Rep. **8** (2018) 56.
[7] P. McCarthy, D. Hwangbo, M. Bilton, S. Kajita and J. W. Bradley: Nuclear Fusion **60** (2020) 026012.
[8] S. Kajita, T. Morgan, H. Tanaka, Y. Hayashi, N. Yoshida, D. Nagata, J. Vernimmen, S. Feng, R. Zhang and N. Ohno: Journal of Nuclear Materials **548** (2021) 152844.
[9] D. Nishijima, M. Baldwin, R. Doerner and J. Yu: Journal of Nuclear Materials **415** (2011) S96.
[10] R. Doerner, M. Baldwin and P. Stangeby: Nucl. Fusion **51** (2011) 043001.
[11] Y. Noiri, S. Kajita and N. Ohno: Journal of Nuclear Materials **463** (2015) 285.
[12] M. Baldwin and R. Doerner: Journal of Nuclear Materials **404** (2010) 165.
[13] S. Takamura and T. Miyamoto: Plasma and Fusion Research **6** (2011) 1202005.
[14] S. Kajita, N. Ohno, M. Yajima and J. Kato: Journal of Nuclear Materials **440** (2013) 55.
[15] G. Wright, G. van Eden, L. Kesler, G. D. Temmerman, D. Whyte and K. Woller: Journal of Nuclear Materials **463** (2015) 294.
[16] T. Petty, M. Baldwin, M. Hasan, R. Doerner and J. Bradley: Nuclear Fusion **55** (2015) 093033.
[17] A. W. Leonard: Physics of Plasmas **21** (2014) 090501.
[18] G. D. Temmerman, R. Doerner and R. Pitts: Nuclear Materials and Energy **19** (2019) 255 .
[19] C.-S. Wong, J. A. Whaley, T. Wada, S. Harayama, Y. Oya and R. D. Kolasinski: Nuclear Materials and Energy **22** (2020) 100730.
[20] T. Okuyama, S. Kajita, N. Yoshida, H. Tanaka, T. Kuwabara and N. Ohno: Plasma and Fusion Research **16** (2021) 1206001.
[21] S. Kajita, N. Yoshida, R. Yoshihara, N. Ohno and M. Yamagiwa: Journal of Nuclear Materials **418** (2011) 152.
[22] S. Kajita, T. Nojima, T. Okuyama, Y. Yamamoto, N. Yoshida and N. Ohno: Acta Materialia **181** (2019) 342.
[23] M. Yajima, N. Yoshida, S. Kajita, M. Tokitani, T. Baba and N. Ohno: Journal of Nuclear Materials **449** (2014) 9.
[24] Y. Gasparyan, V. Efimov and K. Bystrov: Nuclear Fusion **56** (2016) 054002.
[25] K. Woller, D. Whyte and G. Wright: Journal of Nuclear Materials **463** (2015) 289.
[26] R. Doerner, M. Baldwin, M. Simmonds, J. Yu, L. Buzi and T. Schwarz-Selinger: Nuclear Materials and Energy **12** (2017) 372.